Pergamon

Ocean Engng, Vol. 23, No. 2, pp. 167–192, 1996
Elsevier Science Ltd
Printed in Great Britain
0029–8018/96 $15.00 + .00

0029–8018(95)00027-5

A NEW METHOD FOR THE GENERATION OF SECOND-ORDER RANDOM WAVES

Peter Jan van Leeuwen†‡ and Gert Klopman§

†Faculty of Civil Engineering, Technical University Delft, Stevinweg 1, 2628 CN Delft, The Netherlands
§Delft Hydraulics, P.O. Box 152, 8300 AD Emmeloord, The Netherlands

(*Received* 28 *November* 1994; *accepted* 18 *January* 1995)

Abstract—In order to prevent the generation of spurious free sub- and superharmonics of random waves in a laboratory channel, the control signal for the wave board has to be derived according to a higher-order wave theory. An expression for this control signal has been derived with the perturbation method of multiple scales. It is much less complex and requires less computation time than the expressions obtained from the full second-order theory. The new method for second-order subharmonics was verified experimentally for waves with bichromatic and continuous first-order spectra. The data were analysed with the complex-harmonic principal-component analysis to reduce the influence of noise.

1. INTRODUCTION

The generation of realistic non-linear random waves in a flume is important for laboratory experiments in which the problem under investigation is sensitive to second-order effects in the wave field. For instance, second-order subharmonics are important for studies of the surf-beat mechanism, the generation and evolution of sand bars and the slow-drift motion of moored vessels. The second-order superharmonics sharpen the wave crests and flatten the wave troughs and are important for sand transport, among others.

Sand (1982) and Barthel *et al.* (1983) calculated the second-order wave-board motion for the correct generation of the subharmonics, i.e. the bound long waves. They based their work on the transfer function for these low-frequency waves in the absence of a wave board, as first given by Ottesen-Hansen (1978). Sand and Mansard (1986) and Hudspeth and Sulisz (1991) used a similar method for the generation of superharmonics. The transfer function for the superharmonics in the absence of a wave board was given by Dean and Sharma (1981).

The expressions thus obtained for the wave-board control signal are exact to second order. To obtain this signal a convolution-type integral has to be performed. The integration is in the frequency domain and the integrand is a combination of products of the Fourier components of the first-order surface elevation at two different frequencies and the transfer function. In this way the non-linear interactions of all first-order spectral components are taken into account.

‡ Address to which correspondence should be sent: P. J. van Leeuwen, IMAU, University of Utrecht, Princetonplein 5, 3584 CC Utrecht, The Netherlands.

A first look at the resulting equations for the wave-board movement reveals the disadvantage of their use: they are complex, and it requires considerable computing time to obtain a second-order signal for the wave board, mainly due to the convolution. When the first-order spectrum is narrow, this procedure seems unduly expensive. This is because only the frequency components near the peak frequency will give rise to substantial sub- and superharmonics and the transfer function is only slowly varying near the spectral peak frequency.

If the first-order spectrum is narrow, the first-order waves can be described by an oscillation with a slowly modulated frequency and amplitude. This was the motivation to use the method of multiple scales to describe the water motion. The same method was used previously to calculate the second-order waves in the absence of a wave board [e.g. see Mei (1983)]. The modulation acts on a longer time and length scale than the periods and wave lengths of the first-order waves. To incorporate these slow modulations, new time and length scales are introduced to describe these phenomena. So a cascade of new variables is introduced, hence the name of the method.

In this method the calculation of the second-order surface elevations is reduced to a few multiplications in the time domain. In principle, the theory is valid for narrow-banded first-order spectra, but it can even be applied to a Pierson–Moskowitz spectrum. For a detailed discussion of the applicability of this method, the reader is referred to Klopman and Van Leeuwen (1990).

In this paper we derive expressions for the wave-bound control signal for the generation of second-order waves in a channel based on the method of multiple scales. This control signal is such that, in theory, it produces the second-order surface elevations away from the wave board as found by Mei (1983). The use of the multiple-scales method to find the wave-board motion to second order resembles the use of the same method by Agnon and Mei (1985), who determined the slow-drift motion of two-dimensional bodies in beam seas to second order.

The structure of this report is as follows. In Section 2 the method of multiple scales is briefly discussed. The boundary-value problem for the water movement is formulated and the control signal for the wave board is derived. Then in Section 3 the experimental setup is described together with a short explanation of the method of data analysis. This is followed by an experimental test of the new control signal for bichromatic and continuous first-order spectra, described in Section 4. The paper is closed with some conclusions.

2. DERIVATION OF THE CONTROL SIGNAL

In this section the boundary-value problem for the water movement is given followed by a short outline of the method of multiple scales and the resulting expressions for the wave-board movement. Then the control signal for the wave board for the generation of random waves correctly up to second order is derived. Details on the method of multiple scales can be found in Mei (1983), for example; see also Klopman and Van Leeuwen (1990).

2.1. *Problem formulation*

In Fig. 1 a sketch is given of the channel equipped with a wave board. The water depth in absence of waves is h.

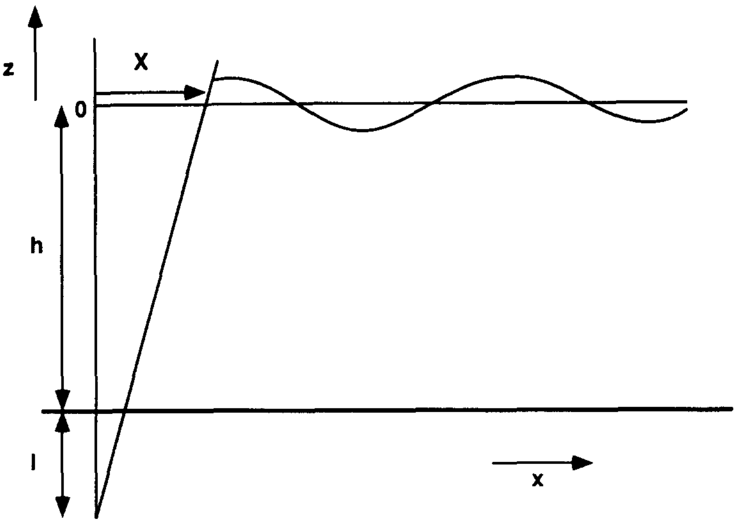

Fig. 1. Definition sketch. h is the water depth, X is the wave-board position on the still water level and $h + l$ is the rotation arm.

We assume that the fluid is inviscid and the basic equations for the velocity potential are the following. The continuity equation reads

$$\Delta\phi = 0 \tag{2.1}$$

in which Δ is the Laplace operator and $\phi(x, z, t)$ the velocity potential. This equation follows from the conservation of mass, with the assumptions of incompressibility and irrotationality. The kinematic free-surface boundary condition reads

$$\zeta_t + \phi_x\zeta_x = \phi_z \text{ on } z = \zeta \tag{2.2}$$

in which $\zeta(x, t)$ is the surface elevation and the lower index indicates partial differentiation to the index variable. Because the surface elevation is not known a priori, we need an extra boundary condition at this boundary. The dynamic free-surface boundary condition is given by the Bernouilli equation

$$g\zeta + \phi_t + \frac{1}{2}(\phi_x^2 + \phi_z^2) = 0 \text{ on } z = \zeta. \tag{2.3}$$

It states that the pressure at the surface is equal to the atmospheric pressure, which is taken as zero here. The boundary condition at the horizontal bottom is given by

$$\phi_z = 0 \text{ on } z = -h \tag{2.4}$$

and states that the velocity of the water particles perpendicular to the bottom is zero. The boundary condition at the wave board reads

$$\phi_x - \frac{\mathrm{d}f}{\mathrm{d}z}X\phi_z = f\frac{\mathrm{d}X}{\mathrm{d}t} \text{ on } x = X, \tag{2.5}$$

in which $X(t)$ is the wave-board position at $z = 0$ and f is given by

$$f(z) = 1 + \frac{z}{h + l},$$

with $l \to \infty$ for a purely translating wave board and $l = 0$ for a purely rotating wave board. Condition (2.5) states that the particle-velocity component normal to the wave board should be equal to the normal component of the wave-board velocity. Finally, far from the wave board the solution must describe the first-order waves with the bound second-order waves as given by Mei (1983). Free second-order waves should not occur.

Because the free-boundary conditions are non-linear, perturbation techniques are used to reduce the non-linear boundary-value problem to a set of linear boundary-value problems. To this end the surface elevation ζ, the velocity potential ϕ and the wave-board position X are expanded in a series in a small non-linearity parameter ϵ, which is equal to the wave steepness.

Because the free surface is part of the problem to be solved it is not known a priori where the boundary condition at the free surface has to be applied. The amplitude of the surface elevation is finite but small, so Taylor series expansions will be carried out at this boundary.

2.2. *The method of analysis*

In this section the method of multiple scales is explained in short. The method is compared briefly with the conventional spectral method to calculate second-order effects.

The objective of the perturbation method is to find expansions for the potential and the surface elevation which are valid for small-but-finite amplitude motions. It is convenient to introduce a small dimensionless parameter ϵ which describes the order of the amplitude of the motion. In our case ϵ is the wave steepness kA, in which k is the wave number and A is the wave amplitude. Next, it is assumed that the wave potential, the surface elevation and the wave-board position can be represented by the following expansions:

$$\phi = \sum_{n=1}^{\infty} \epsilon^n \phi_n \tag{2.6}$$

$$\zeta = \sum_{n=1}^{\infty} \epsilon^n \zeta_n \tag{2.7}$$

$$X = \sum_{n=1}^{\infty} \epsilon^n X_n . \tag{2.8}$$

The expansions are substituted in the basic equations (2.1)–(2.5). Because ϕ_n, ζ_n and X_n are independent of ϵ, the coefficients for each power of ϵ are set equal to zero. This leads to n sets of linear equations, one for each order. Of course ϕ_n/ϕ_{n-1} must be bounded in order to have a consistent perturbation scheme.

In the conventional spectral methods the first-order quantities ζ_1 and ϕ_1 are decomposed into Fourier series of the form

$$\zeta_1 = \sum_{n=0}^{N} \zeta_{1_n} e^{-i\omega_n t}. \tag{2.9}$$

Then the Fourier series of the second-order quantities ζ_2 and ϕ_2 are found from the second-order equations. In this way the non-linear interactions of all first-order Fourier components are taken into account to obtain the second-order Fourier components. This results in complex expressions for the second-order quantities, especially for the wave-board motion. A way to decrease the number of calculations is to take only those non-linear interactions into account which occur between first-order Fourier components which contain more energy than a certain minimum. However, the resulting equations are still complex.

In the case of a narrow first-order spectrum, a stronger assumption can be used. The assumption is that ζ_1 varies sinusoidally with a modulated amplitude and frequency. However, two problems occur when the straightforward expansions from Equations (2.6)–(2.8) are used in the governing equations.

Firstly, the solution turns out to have a limited range of validity. So-called secular terms, such as $\epsilon t \sin\omega t$, appear in the second-order terms. Thus, it can be seen that ϕ_n/ϕ_{n-1} is not bounded as t increases, which means that the expansion is not uniformly valid as t increases. The problem arises from the fact that the (angular) frequency ω is wave-amplitude-dependent in a non-linear system. A possible way to circumvent this problem is to introduce new variables describing slow-scale changes which take care of the frequency changes. These new variables are used to eliminate the secular terms by imposing so-called solvability conditions, which ensure that the expansions are uniform (see e.g. Nayfeh, 1981).

Secondly, non-linear interactions of a sinusoidal wave with itself will only produce superharmonics in the straightforward expansion, while subharmonics are clearly present in nature. Also here the introduction of new variables, describing different time and length scales, will solve the problem.

In the method of multiple scales the expansions for the velocity potential, the surface elevation and the wave-board position are considered to be functions of multiple independent variables, or scales. These new variables are introduced as

$$t_n = \mu^n t \tag{2.10}$$

$$x_n = \mu^n x\,, \tag{2.11}$$

in which μ is a small parameter which describes the modulation of the first-order wave amplitude. So the variables with $n > 0$ will describe the slow modulation of the primary-wave amplitude and will be called slow variables hereafter. Because the slow variables will be used to describe the wave-amplitude variations, μ will be of the order wave period over group period. The derivatives with respect to x and t become

$$\frac{\partial}{\partial t} = \frac{\partial}{\partial t_0} + \mu\frac{\partial}{\partial t_1} + O(\mu^2)$$

$$\frac{\partial}{\partial x} = \frac{\partial}{\partial x_0} + \mu\frac{\partial}{\partial x_1} + O(\mu^2) \tag{2.12}$$

so that a derivative to a slow variable is of a lower order than a derivative to a fast variable. In the following, the index 0 will be omitted for brevity.

In the case of a narrow-banded energy–density spectrum of the primary waves, the method of multiple scales can be applied. The assumption is that the water surface oscillates with the peak frequency of the spectrum with a modulated wave amplitude and frequency. The second-order effects arise from the non-linear interactions of the primary waves. The second-order superharmonics have twice the frequency of the primary waves, and produce sharper peaks and flatter troughs and thus give rise to wave asymmetry. The second-order subharmonics arise from the wave-amplitude modulations and appear as long waves bound to wave groups.

Motivated by the multiple scales, we introduce the following notation:

$$\zeta_n(x,z,t) = \sum_{m=-n}^{m=n} \zeta_{nm}(x_0, x_1, t_1, x_2, t_2, \dots)\, \mathrm{e}^{-im\omega t}, \tag{2.13}$$

in which ω is the angular frequency of the first-order waves and $\zeta_{n,-m} = \zeta^*_{n,m}$ to keep ζ_n real. An asterisk superscript denotes the complex conjugate of the term. Note that ζ_{nm} depends only on the slow variables. A similar notation will be used for ϕ_n and X_n.

As the solution method is posed so far, two small parameters are introduced, ϵ and μ. In order to simplify the problem, these two parameters will be related. A standard way to do this in perturbation analysis is

$$\mu = \epsilon^{\lambda}, \tag{2.14}$$

in which λ is a parameter of order one. We will assume

$$\lambda = 1, \tag{2.15}$$

so the wave steepness is equal to the modulation parameter. A motivation for this choice comes from the characteristic shape of the first-order spectrum which we usually encounter, such as JONSWAP spectrum or a Pierson–Moskowitz spectrum. For such a spectrum the magnitude of the parameter μ can be taken as a dimensionless spectral-width parameter. As the magnitude of ϵ we can take the product of the wave number at the peak frequency and half the significant wave height. If we choose these values for the parameters, they are of the same order of magnitude.

Now that the slow time and length scales are introduced together with the perturbation series for the potential, the surface elevation and the wave-board motion, the first- and second-order boundary-value problems can be formulated and solved.

2.3. *First-order solution*

The perturbation series for the wave potential, the surface elevation and the wave-board displacement plus the fast and slow time scales are incorporated in Equations (2.1)–(2.5). Then a Taylor series expansion of the free-surface boundary conditions is carried out in the vertical direction around $z = 0$, and of the wave-board boundary conditions in the horizontal direction around $x = 0$. The expansions lead to the following first-order problem:

$$\Delta\phi_1 = 0 \tag{2.16}$$

$$\phi_{1_{tt}} + g\phi_{1_z} = 0 \qquad \text{on } z = 0 \tag{2.17}$$

$$\phi_{1_z} = 0 \qquad \text{on } z = 0 \tag{2.18}$$

$$\phi_{1_x} = f(z)\frac{\mathrm{d}X_1}{\mathrm{d}t} \qquad \text{on } x = 0 \tag{2.19}$$

with

$$\zeta_1 = -\frac{1}{g}\phi_{1_t} \qquad \text{on } z = 0\,. \tag{2.20}$$

To solve the first-order problem we use as a further input that the first-order surface elevation far from the wave board is given by

$$\zeta_1 = \frac{1}{2}(A\mathrm{e}^{i\psi} + {}^*) = \zeta_{11}\mathrm{e}^{-i\omega t} + \zeta_{11}^*\mathrm{e}^{i\omega t} \qquad \text{for } x \to \infty\,, \tag{2.21}$$

in which $\psi = kx - i\omega t$, $A = A(t_1, x_1)$ is the complex amplitude of the first-order waves. The magnitude $|A|$ of A is equal to the envelope of the surface elevation in a time simulation based on the first-order energy–density spectrum which we want to have in the channel. The asterisk denotes the complex conjugate of the preceding term. Note that we used the notation defined in Equation (2.13).

Suppose the wave-board position is given by

$$X_{11} = ia\,, \tag{2.22}$$

in which $a(t_1)$ is the slowly varying amplitude of the wave-board stroke. Although X_{10} is a first-order quantity, it does not show up in the first-order problem because the wave-board position is differentiated to a fast variable [see Equation (2.19)] and X_{10} only depends on the slow variables. It will produce the subharmonics as we will see in the second-order problem.

Biésel (1952) found the solution to the first-order problem as

$$\phi_{11} = -B\frac{\cosh Q}{\cosh q}ia\mathrm{e}^{ikx} + \sum_{j=1}^{\infty} C_j\frac{\cos P_j}{\cos p_j}\mathrm{e}^{-l_jx}a\,, \tag{2.23}$$

in which

$$B = \frac{2\omega}{k(\mathrm{sh}\,2q + 2q)}\left[\mathrm{sh}\,2q - \frac{2\mathrm{ch}^2\,q}{k(h+l)}\right] \tag{2.24}$$

$$C_j = -\frac{2\omega}{l_j(\sin 2p_j + 2p_j)}\left[\sin 2p_j - \frac{2\cos^2 p_j}{l_j(h+l)}\right] \tag{2.25}$$

with

$$Q = k(z+h) \quad P_j = l_j(z+h) \quad q = kh \quad p_j = l_jh\,,$$

$$n = \frac{1}{2} + \frac{q}{\sinh(2q)} \quad n_j = \frac{1}{2} + \frac{p_j}{\sin(2p_j)}\,. \tag{2.26}$$

k is the positive and real root of $\omega^2 = gk\tanh kh$ and l_j is the positive and real root of $-\omega^2 = gl_j\tan l_jh$ with $(j - \frac{1}{2})\pi < l_jh \le j\pi$ for $j = 1, 2, 3, \ldots$.

Note that ϕ_{10} does not show up in the first-order solution because it only depends on the slow variables. It was shown by Mei (1983, p. 615) to represent the bound low-frequency waves, arising from the amplitude modulation of the primary waves. It will show up in the second-order problem.

The first-order surface elevation can be calculated from Equation (2.20) as

$$\zeta_{11} = \frac{\omega B}{2g} e^{ikx} a + \frac{\omega}{2g} \sum_{j=1}^{\infty} C_j e^{-l_j x} \, ia \tag{2.27}$$

and

$$\zeta_{10} = 0\,. \tag{2.28}$$

The first term on the right-hand-side of Equation (2.27) represents the progressive waves and the second term represents the evanescent modes. We will elaborate on these waves shortly. First we identify the quantity a.

Far from the wave board, where only progressive waves are present because the evanescent modes have died out, ζ_{11} should satisfy Equation (2.21):

$$\zeta_{11} = \frac{1}{2} A e^{ikx}\,, \tag{2.29}$$

so that using (2.27) far from the wave board we can identify

$$a = \frac{gA}{\omega B}\,. \tag{2.30}$$

The first-order wave-board position is now given by

$$X_{11} = \frac{g}{2\omega B} iA \tag{2.31}$$

and the first-order potential becomes

$$\phi_{11} = -\frac{g}{2\omega} \frac{\cosh Q}{\cosh q} iA e^{ikx} + \frac{g}{2\omega} \sum_{j=1}^{\infty} \frac{C_j}{B} \frac{\cos P_j}{\cos p_j} e^{-l_j x} A\,. \tag{2.32}$$

The first term on the right in Equation (2.32) is identical to that obtained by Mei (1983, p. 611). It represents the free waves travelling in the positive x-direction. The second term describes standing waves in the z-direction, with amplitudes decaying in the x-direction, the so-called evanescent modes. They arise because the wave board does not produce the correct velocity profile over the water depth, but only an approximation. So the progressive waves produced by the wave board do not fulfil the boundary condition exactly. Evanescent modes are generated so that the sum of the progressive waves and the evanescent modes fulfils the boundary condition to first order. The influence of the wave-board boundary condition is via the factors B and C_j, which indeed only occur in the second term.

The first-order surface elevation becomes

$$\zeta_{11} = \frac{1}{2}Ae^{ikx} + \frac{1}{2}\sum_{j=1}^{\infty}\frac{C_j}{B}e^{-l_jx}\,iA\,. \tag{2.33}$$

2.4. *Second-order solution*

We now consider the second-order problem and solution. We solve for the harmonic components separately to keep the work surveyable. First we treat the second-order first-harmonic case, then the second-order superharmonic case and finally the second-order subharmonic problem.

2.4.1 *The second-order first-harmonic solution.* The governing equations for the second-order first-harmonic potential are

$$\Delta\phi_{21} = -2\phi_{11_{xx_1}} \tag{2.34}$$

$$-\omega^2\phi_{21} + g\phi_{21_z} = 2i\omega\phi_{11_{t_1}} \qquad \text{on } z = 0 \tag{2.35}$$

$$\phi_{21_z} = 0 \qquad \text{on } z = 0 \tag{2.36}$$

$$\phi_{21_x} = -i\omega f(z)X_{21} + f(z)X_{11_{t_1}} - \phi_{11_{x_1}} - f(z)X_{10}\phi_{11_{xx}} + \frac{X_{10}\phi_{11_z}}{h+l} \qquad \text{on } x = 0\,. \tag{2.37}$$

The solution to Equations (2.34) and (2.36) is given by

$$\phi_{21} = D\,\mathrm{ch}\,Q e^{ikx} + \Sigma_j E_j \cos P_j e^{-l_jx} - \frac{g}{2\omega k}\frac{Q\,\mathrm{sh}\,Q}{\mathrm{ch}\,q}\frac{\partial A}{\partial x_1}e^{ikx} + \frac{g}{2\omega}\Sigma_j\frac{C_j}{B\cos p_j}\left[\lambda_j\frac{P_j\sin P_j}{l_j} + x(\lambda_j - 1)\cos P_j\right]e^{-l_jx}\frac{\partial A}{\partial x_1}\,. \tag{2.38}$$

The constants D, E_j and λ_j are determined below. The term with the factor xe^{-l_jx} has not been published before and was overlooked by Hudspeth and Sulisz (1991). However, because this term vanishes at the wave board and far from the wave board, it does not contribute to the second-order wave-board control signal. At third order this term will be important. Note that terms which contain the factor xe^{ikx} are unphysical because they give rise to an infinite growth of ϕ_{21_x} as x increases.

Far from the wave board we choose the corresponding surface elevation to be zero. (Note that we do have this freedom in the second-order problem.) The advantage of this choice is that the spectral density of the waves with frequencies close to the peak frequency of the energy–density spectrum is determined by the first-order waves only. We thus find far from the wave board:

$$\zeta_{21} = \frac{i\omega}{g}\phi_{21} - \frac{1}{g}\phi_{11_{t_1}} = 0 \quad \text{for } x \to \infty. \tag{2.39}$$

This equation is fulfilled when

$$D = \frac{gq\,\mathrm{th}\,q}{2k\omega\mathrm{ch}\,q}\frac{\partial A}{\partial x_1} - \frac{g}{2\omega^2\mathrm{ch}\,q}\frac{\partial A}{\partial t_1}. \tag{2.40}$$

To find λ_j we use Equation (2.35). This equation can be rewritten as

$$g\left(\frac{\partial A}{\partial t_1} + C_g\frac{\partial A}{\partial x_1}\right)e^{ikx} + g\,\Sigma_j\frac{C_j}{B}\left(i\frac{\partial A}{\partial t_1} + \frac{\partial\omega}{\partial l_j}\lambda_j\frac{\partial A}{\partial x_1}\right)e^{-l_j x} = 0 \tag{2.41}$$

in which C_g is the group velocity given by $C_g = \dfrac{\partial\omega}{\partial k}$.

Because A is independent of x_0, one has

$$\frac{\partial A}{\partial t_1} + C_g\frac{\partial A}{\partial x_1} = 0 \tag{2.42}$$

and

$$i\frac{\partial A}{\partial t_1} + \frac{\partial\omega}{\partial l_j}\lambda_j\frac{\partial A}{x_1} = 0\,. \tag{2.43}$$

The first equation shows that the energy-transfer velocity is the group velocity C_g; the second equation determines λ_j as

$$\lambda_j = iC_g\left(\frac{\partial\omega}{\partial l_j}\right)^{-1}. \tag{2.44}$$

The determination of the constants E_j is a little more complex. It is found from a solvability condition on ϕ_{21}, which is equal to Green's theorem on ϕ_{11} and ϕ_{21} in this case [see for instance Foda and Mei (1981)]. It reads

$$\int_{-h}^{O}\int_0^L(\phi_{11}\Delta\phi_{21} - \phi_{21}\Delta\phi_{11})\,\mathrm{d}x\mathrm{d}z = \int_{-h}^{0}[\phi_{11}\phi_{21_x} - \phi_{21}\phi_{11_x}]_{x=0}\,\mathrm{d}z + \frac{2i\omega}{g}\int_0^L[\phi_{11}\phi_{11_{t_1}}]_{z=0}\,\mathrm{d}x \tag{2.45}$$

in which L denotes a position far from the wave board where the evanescent modes have died out. When the equations for ϕ_{11} and ϕ_{21} are used in this equation, we obtain for the constants E_j:

$$E_j = \frac{g\lambda_j}{2\omega\cos p_j}\left(\Sigma_i\frac{C_i}{B(l_i + l_j)} - \frac{C_j}{2Bl_j}\right)\frac{\partial A}{\partial x_j}. \tag{2.46}$$

Now that we have found the complete solution for ϕ_{21}, we can determine the wave-board motion X_{21} from Equation (2.37). This equation is integrated over depth to obtain

$$X_{21} = -\frac{i}{\omega}X_{11_{t_1}} + \frac{iR}{\omega}\left[\int_{-h}^{0}\phi_{21_x}\,\mathrm{d}z + \int_{-h}^{0}\phi_{11_{x_1}}\,\mathrm{d}z - \frac{\omega^2}{g}X_{10}\phi_{11}\,(z=0)\right] \tag{2.47}$$

in which we introduced the constant R which is given by

$$R = \frac{2h + 2l}{h + 2l}. \tag{2.48}$$

Note that $R = 1$ for a purely translating wave board. We can evaluate this equation as

$$X_{21} = \left[\frac{g}{2\omega^2 B} - \frac{gR}{2\omega^2 C_g} \left(1 + \sum_{j=1}^{\infty} \left[C_j \lambda_j \left(1 + \frac{\tan p_j}{2p_j} \right) \right. \right. \right. \tag{2.49}$$

$$\left. \left. \left. - \lambda_j \tan p_j \sum_{i=1}^{\infty} \frac{C_j}{p_j + p_i} \right] \right) \right] \frac{\partial A}{\partial t_1} - \frac{RX_{10}}{2h} \left(1 + i \sum_{j=1}^{\infty} C_j \right) A .$$

The first term in this equation describes the frequency modulation; it is proportional to $\partial A/\partial t_1$. The second term contains the slow wave-board motion X_{10}. An expression for this quantity will be given below.

2.4.2. *The superharmonic solution.* The governing equations for the superharmonic second-order potential are

$$\Delta\phi_{22} = 0 \tag{2.50}$$

$$-4\omega^2\phi_{22} + g\phi_{22} = 3i\frac{\omega^5}{g^2}\phi_{11}^2 + 2i\omega\phi_{11_x}^2 + i\omega\phi_{11}\phi_{11_{xx}} \tag{2.51}$$

$$\phi_{22_z} = 0 \tag{2.52}$$

$$\phi_{22_x} = -2i\omega f(z)X_{22} - f(z)X_{11}\phi_{11_{xx}} + X_{11}\frac{\phi_{11_z}}{h + l}. \tag{2.53}$$

The solution to (2.50) and (2.52) is given by

$$\phi_{22} = \tilde{D}\operatorname{ch}\tilde{Q}e^{i\tilde{k}x} + \Sigma_j \tilde{E}_j \cos\tilde{P}_j e^{-\tilde{l}x} + F\operatorname{ch}2Q\, e^{2ikx}$$
$$+ \Sigma_j G_j \cos(P_j - iQ)e^{(ik - l_j)x} + \Sigma_{ij} H_{ij}\cos(P_i + P_j)\, e^{-(l_i + l_j)x}. \tag{2.54}$$

The variables with the tildes contain the wave numbers which follow from the dispersion relations for free waves:

$$4\omega^2 = g\tilde{k}\tanh h\tilde{k} \tag{2.55}$$

and

$$-4\omega^2 = g\tilde{l}_j \tan h\tilde{l}_j. \tag{2.56}$$

Because we want all superharmonics to be bound waves, the coefficients $\tilde{D}$ and $\tilde{E}_j$ are set equal to zero. The coefficients F, G_j and H_{ij} can be found from Equation (2.51) as:

$$F = -\frac{3}{16}\frac{\omega}{\operatorname{sh}^4 q} iA^2 \tag{2.57}$$

$$G_j = -\frac{1}{4\omega}\frac{C_j}{B}\frac{(6\omega^4 - 4ig^2kl_j - g^2k^2 + g^2l_j^2)}{4\omega^2\cos(p_j - iq) + g(l_j - ik)\sin(p_j - iq)}A^2 \tag{2.58}$$

$$H_{ij} = -\frac{1}{4\omega}\frac{C_iC_j}{B^2}\frac{(3\omega^4 + 2g^2l_il_j + g^2l_j^2)}{4\omega^2\cos(p_i + p_j) + g(l_i + l_j)\sin(p_i + p_j)}iA^2 . \tag{2.59}$$

Now that we have found the full solution for the second-order superharmonic potential we derive the corresponding wave-board motion. To this end Equation (2.53) is integrated over the depth to obtain

$$\int_{-h}^{0}\phi_{22_x}\,dx = -2i\omega X_{22}\int_{-h}^{0}f(z)dz - X_{11}\int_{-h}^{0}f(z)\phi_{11_{xx}}\,dz + X_{11}\int_{-h}^{0}\frac{\phi_{11_z}}{h+l}dz . \tag{2.60}$$

The last two terms can be evaluated to give

$$X_{22} = \frac{iR}{2\omega h}\left[\int_{-h}^{0}\phi_{22_x}\,dz - \frac{\omega^2}{g}X_{11}\phi_{11}(z=0)\right]. \tag{2.61}$$

This can be evaluated as

$$\begin{aligned} X_{22} = \frac{iR}{2\omega h}\Bigg[&\left(\frac{3}{4}\frac{gk}{\omega \mathrm{sh}^2 q} - \frac{g}{4B}\right)A^2 - \frac{g}{4}\Sigma_j\frac{C_j}{B^2}iA^2 \\ &+ \frac{1}{4\omega}\Sigma_j\frac{C_j}{B}\frac{(6\omega^4 - 4g^2kl_j - g^2k^2 + g^2l_j^2)}{4\omega^2\tan^{-1}(p_j - iq) + g(l_j - ik)}A^2 \\ &+ \frac{1}{4\omega}\Sigma_{ij}\frac{C_iC_j}{B^2}\frac{(3\omega^4 + 2g^2l_il_j + g^2l_j^2)}{4\omega^2\tan^{-1}(p_i + p_j) + g(l_i + l_j)}iA^2\Bigg]. \end{aligned} \tag{2.62}$$

Let us now turn to the subharmonic problem.

2.4.3. *The subharmonic problem.* In this section we solve the boundary-value problem for the second-order subharmonic wave-board motion. The subharmonic wave generation is relatively easy to handle because the subharmonic waves far from the wave board have no z-dependence, so the equations can be integrated over the depth.

The boundary-value problem for ϕ_{10} is given by

$$\Delta\phi_{10} = 0 \tag{2.63}$$

$$\phi_{10_z} = 0 \qquad \text{on } z = 0 \tag{2.64}$$

$$\phi_{10_z} = 0 \qquad \text{on } z = -h \tag{2.65}$$

$$\phi_{10_x} = 0 \qquad \text{on } x = 0 . \tag{2.66}$$

The solution to this problem is that ϕ_{10} does not depend on the fast variables. We need higher-order equations to determine the dependence of ϕ_{10} on the slow variables. Let us now have a look at the problem for ϕ_{20}.

The boundary-value problem for ϕ_{20} reads

$$\Delta\phi_{20} = 0 \tag{2.67}$$

$$\phi_{20_z} = (\zeta_{11}\phi_{11_x} + {}^*)_x \qquad \text{on } z = 0 \tag{2.68}$$

$$\phi_{20_z} = 0 \qquad \text{on } z = -h \tag{2.69}$$

$$\phi_{20_x} = X_{10_{t_1}} - \phi_{10_{x_1}} - (X^*_{11}\phi_{11_{xx}} + {}^*)\,. \quad \text{on } x = 0\,. \tag{2.70}$$

This last equation can immediately be integrated to

$$\int_{-h}^{0} \phi_{20_x}\,\mathrm{d}z = \frac{1}{R} X_{10_{t_1}} - h\phi_{10_{x_1}} - (\zeta_{11}\overset{*}{\phi}_{11_x} + {}^*) \qquad \text{on } x = 0\,, \tag{2.71}$$

in which we used Equations (2.16)–(2.19). An easy way to find X_{10} is to ignore the solution for ϕ_{20} and start from the continuity equation. It reads after integration over depth:

$$\zeta_t + [(h + \zeta)U]_x = 0\,, \tag{2.72}$$

in which U is the depth averaged velocity given by

$$U = \frac{1}{h + \zeta}\int_{-h}^{\zeta} \phi_x\,\mathrm{d}z\,.$$

The second-order subharmonic continuity equation is given by

$$\int_{-h}^{0} \phi_{20_x}\,\mathrm{d}z + (\zeta_{11}\overset{*}{\phi}_{11_x} + {}^*) = C\,. \tag{2.73}$$

Note that $\zeta_{10_{t_1}} = 0$ from Equation (2.20). C depends on the slow variables and is determined by the fact that far from the wave board the subharmonic velocity potentials describe the bound low-frequency waves which are not dependent on the fast variable x. So, far from the wave board ϕ_{20_x} must vanish and we find

$$C = (\zeta_{11}\overset{*}{\phi}_{11_x} + {}^*)_{x=L}\,, \tag{2.74}$$

in which $x = L$ denotes a place far from the wave board where the evanescent modes have died out. The same equation can be found via Green's theorem for ϕ_{10} and ϕ_{20} [see Agnon and Mei (1985)].

If we combine Equations (2.71), (2.73) and (2.74), we find for the wave-board motion

$$X_{10_{t_1}} = R\left[\phi_{10_{x_1}} + \frac{1}{h}(\zeta_{11}\overset{*}{\phi}_{11_x} + {}^*)_{x=L}\right]. \tag{2.75}$$

Note that we did not have to solve for ϕ_{20}. Via the continuity equation we are able to link the wave-board position to the variables far from the wave board. Recall that ϕ_{10} does not depend on the fast variables. This result can be interpreted as that the evanescent modes give rise to low-frequency motion close to the wave board which are described by the part of ϕ_{20} depending on the fast space coordinate.

Now we will replace ϕ_{10} by ζ_{20} in Equation (2.75). To do this we need the third-order subharmonic continuity equation far from the wave board, where the evanescent modes have died out. It is given by

$$\zeta_{20_{t_1}} + h\phi_{10_{x_1x_1}} + (\zeta_{11}\phi^*_{11_x} + {}^*)_{x_1} = 0\,. \tag{2.76}$$

The surface elevation ζ_{20} describes the bound waves and the propagation velocity of these waves is the group velocity of the first-order waves C_g. We thus have

$$\zeta_{20_{t_1}} = -C_g\,\zeta_{20_{x_1}}\,. \tag{2.77}$$

With this equation the continuity equation (2.76) can be integrated with respect to x_1 to obtain

$$C_g\,[\zeta_{20} - S_1] = h\phi_{10_{x_1}} + (\zeta_{11}\phi^*_{11_x} + {}^*) \tag{2.78}$$

in which S_1 is an integration constant. The wave-board motion can now be expressed with Equation (2.75) as

$$X_{10_{t_1}} = R\,\frac{C_g}{h}\,[\zeta_{20} - S_1]\,. \tag{2.79}$$

This equation can be integrated to obtain the control signal for the wave board:

$$X_{10} = R\,\frac{C_g}{h}\int_0^{t_1}(\zeta_{20} - S_1)\,\mathrm{d}t_1\,, \tag{2.80}$$

and the constant S_1 is found by demanding that the wave-board stroke remains finite:

$$S_1 = \overline{\zeta_{20}}\,, \tag{2.81}$$

where the bar indicates the value of the quantity averaged over t_1. The equation for the wave-board motion (2.80) states that the volume flux due to this motion produces the surface elevation of the low-frequency waves, just as one would expect.

An expression for ζ_{20} can be found from the boundary-value problem for ϕ_{30} or from the second-order Bernoulli equation. We will use the last method because its physical relevance is more clearly understood. The Bernoulli equation on the free surface reads

$$g\zeta + \phi_t + \frac{1}{2}(|\phi_x|^2 + |\phi_z|^2) = 0 \qquad \text{on } z = \zeta\,. \tag{2.82}$$

The second-order subharmonic version of this equation reads

$$g\zeta_{20} + \phi_{10_{t_1}} + |\phi_{11_x}|^2 - \frac{\omega^4}{g^2}|\phi_{11}|^2 = 0 \qquad \text{on } z = 0\,. \tag{2.83}$$

To obtain this equation we made use of the first-order kinematic and dynamic free-surface boundary conditions and a Taylor expansion around $z = 0$. The third-order subharmonic continuity equation was given by:

$$\zeta_{20_{t_1}} + h\phi_{10_{x_1x_1}} + (\zeta_{11}\phi^*_{11_x} + {}^*)_{x_1} = 0\,.$$

Now we use the fact that the bound subharmonic waves travel with the group velocity C_g of the first-order waves and eliminate the velocity potential ϕ_{10} by substitution of Equation (2.83), and the use of Equation (2.77) and a similar equation for ϕ_{10}. We then find for the surface elevation

$$\zeta_{20} = \frac{1}{gh - C_g^2}\left[h|\phi_{11_x}|^2 - \frac{\omega^4 h}{g^2}|\phi_{11}|^2 - C_g(\zeta_{11}\phi^*_{11_x} + {}^*)\right]. \tag{2.84}$$

The right-hand side can be evaluated with help of the expressions for the first-order quantities to obtain

$$\zeta_{20} = -\frac{g(2n - \frac{1}{2})|A|^2}{gh - C_g^2} \tag{2.85}$$

in which n is given by Equation (2.26). This equation can be written as

$$\zeta_{20} = \frac{S}{\rho(gh - C_g^2)} \tag{2.86}$$

in which S is the radiation stress of the first-order waves. This equation was first obtained by Longuet-Higgins and Stewart (1962). If we use this in Equation (2.80) for the slow wave-board motion we obtain

$$X_{10} = R\frac{gC_g\left(2n - \frac{1}{2}\right)}{h(gh - C_g^2)}\int_0^{t_1}(|A|^2 - \overline{|A|^2})\,\mathrm{d}t_1. \tag{2.87}$$

An important remark has to be made here. From Equation (2.87) one can get the impression that X_{10} is of second-order magnitude because it is proportional to $|A|^2$. However, due to the integration with respect to t_1 the magnitude of this term is first-order. (Its magnitude is of order ϵ^2/μ.)

The total control signal for random wave generation up to second order now becomes

$$X(t,t_1) = X_{11}(t_1)\,\mathrm{e}^{-i\omega t} + X_{10}(t_1) + X_{21}(t_1)\,\mathrm{e}^{-i\omega t} + X_{22}(t_1)\,\mathrm{e}^{-2i\omega t} + {}^*. \tag{2.88}$$

The quantities on the right-hand side are found in Equations (2.31), (2.49), (2.62) and (2.87).

2.5. *Implementation*

Now that we have obtained the control signal for the wave board up to second order, we will give the recipe for the generation of the complete control signal.

Firstly, the peak frequency of the given first-order energy–density spectrum has to be determined. At this frequency the wavenumber k, the group velocity C_g and the quantities q and p_j (given in Equation 2.26) have to be calculated.

Secondly, a time series for the required first-order surface elevation ζ_{11} has to be generated from the given first-order energy-density spectrum. In this way $A(t_1)$ is determined. We used the random-amplitude/random-phase method described by Tucker *et al.* (1984).

Thirdly, the control signal for the wave board has to be calculated in the time domain from Equation (2.88). We perform the time integration in Equation (2.87) with the modified midpoint rule and the time differentiations with central differences. The accuracy of both operations is second order.

These three steps are sufficient to obtain the control signal for the wave board correct up to second order. To obtain this signal with our narrow-banded approximation method, an FFT and a few extra multiplications have to be performed. In the frequency-domain exact methods an FFT, a few extra multiplications and a convolution are needed. An FFT needs $4pN$ multiply–add operations in which N is the number of time steps and $p = {}^2\log N$ [see for instance Bendat and Piersol (1986)]. For the convolution in the frequency-domain methods N^2 operations are needed, as can be observed in Barthel *et al.* (1983) and Sand and Mansard (1986). If we neglect the extra multiplications (of which more are needed in the frequency-domain approach) the gain in computational speed of the new method compared to the conventional method is

$$\frac{4pN + N^2}{4pN} = 1 + \frac{N}{4p}.$$

In a typical experiment N will be of the order of 10^4 or more, so that the gain in speed is of the order of 100.

Note that the equations can also be used to generate second-order monochromatic and bichromatic waves.

3. EXPERIMENTS

3.1. *Experimental arrangement*

To verify the theory, experiments were conducted in a wave channel of length 40 m and width 0.8 m. At 19 m from the wave board a 1:25 concrete slope started (see Fig. 2). In one experiment a concrete bar of height 10 cm was placed on the sloping bottom. This bar has a Gaussian shape. The channel is equipped with a hydraulically driven wave board operating in translatory mode.

The experiments were performed with bichromatic and continuous first-order spectra. In the case of the bichromatic energy–density spectrum of the first-order waves, four wave-height meters were placed at distances of respectively 10, 14, 16 and 18 m from the mean wave-board position. The reflection of the beach was reduced by absorbing material on the water line to be able to concentrate fully on the generation. The still-water depth was 0.50 m and the sample frequency was 50 Hz.

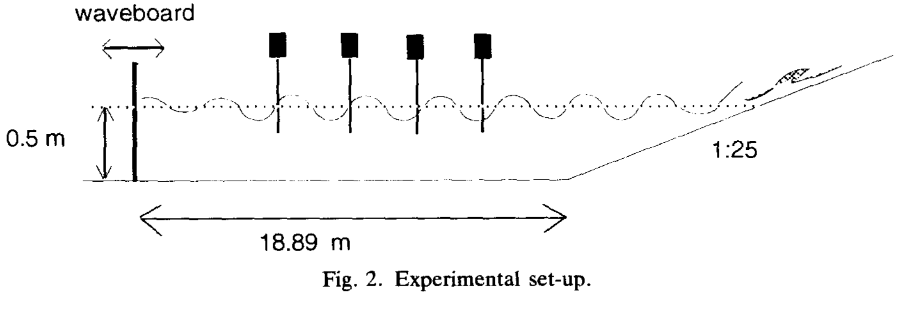

Fig. 2. Experimental set-up.

In the case of the continuous first-order spectra six wave-height meters were used at respectively 6, 10, 12, 14, 15 and 18 m from the mean wave-board position. The absorbing material on the water line was not present. The still-water depth was 0.42 m and the sample frequencies were 10 and 20 Hz.

3.2. *Reflection on the wave board*

To avoid re-reflection of waves against the wave board, it is equipped with an active wave-absorption system. Wave-height meters are fixed to the wave board, which measure the instantaneous water-surface elevation on the board. This signal is integrated in time to obtain a wave-board position. This position is then compared with the previously calculated position and the difference is compensated for by an extra movement of the wave board. In this way waves which are reflected from the beach are absorbed. This absorption system has been used successfully by Kostense (1984).

We performed a test of this absorption system. To this end the slope was replaced by a vertical wall 38 m from the wave board. The reflection coefficient of the wave board at a range of frequencies was determined. This coefficient was obtained in the following way. The wave board produced waves of a certain frequency until a steady situation occurred with standing waves. A wave-height meter was placed at a surface-elevation amplitude maximum and this maximum was recorded. Then the absorption system was switched on. The amplitude of the standing waves was recorded again when waves, which were partially reflected by the wave board, were reflected on the vertical wall and reached the wave-height meter again. At that moment the waves coming from either side were both partially absorbed by the wave board once. The reflection coefficient is given by the ratio of latter to the former recorded amplitude.

In Fig. 3 the variation of the reflection coefficient as function of frequency is given.

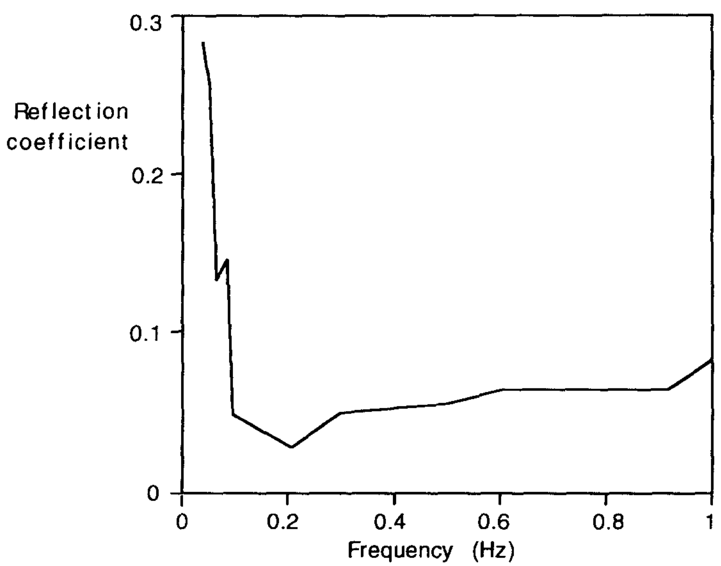

Fig. 3. Reflection coefficient of the wave board with active wave absorption as a function of frequency.

For frequencies higher than 0.1 Hz the reflection coefficient is well below 10%, which is acceptable for our purpose. High-frequency waves will break on the beach and their reflection back to the wave board will be very small. Low-frequency waves will reflect nearly 100% on the beach, but are of second order. The reflection at the wave board will reduce them to third order and we want to test the second-order theory.

A problem is formed by the waves with frequencies lower than about 0.05 Hz. The reflection coefficient of the wave board is too high in this case. It means that these waves are re-reflected by the wave board and will travel to the beach again. Of course, this does not happen on a natural beach. The reason for this high reflection is probably leakage of water below and along the sides of the wave board. In our case it means that we can only test the model down to 0.05 Hz. However, for instance surf-beat phenomena are usually above this frequency (at the used laboratory scale).

3.3. *Data processing*

The data are Fourier transformed and the influence of noise which is uncorrelated with the wave signals is reduced by means of complex harmonic principal component analysis (CHPCA). This last method was developed by Wallace and Dickinson (1972) and has been widely used in meteorology and oceanography. Recently, the method found its way in coastal engineering. An example of this is given by Tatavarti *et al.* (1988), who showed with CHPCA that the reflection coefficient of low-frequency waves can easily be overestimated when using standard cross-spectral analysis, because noise tends to push the reflection coefficient to one.

The idea behind the method is that the wave signals and the noise signals are uncorrelated. This means that the noise does not show up in the quadrature spectra of the different sensors. However, noise does show up in the coincident spectra. In the CHPCA the quadrature spectra are used to reduce the influence of noise in the coincident spectra. For more details about this method, the reader is referred to Preisendorfer (1988) and the articles mentioned above.

The resulting low-frequency wave signals were split into outgoing bound, outgoing free and incoming free waves. ("Outgoing" and "incoming" means travelling from and towards the wave board, so we observe the system from the wave board.) This decomposition makes use of the difference in wavenumber or in phase speed of different low-frequency waves. For the bound waves this phase speed is C_g, the group velocity of the first-order waves. The free waves both have a phase velocity of $\sqrt{gh}$, but of opposite sign.

3.4. *Noise level and error analysis*

The noise level and the error analysis need special attention. In the bichromatic case, we found from parts of the low-frequency spectrum in which no energy was present theoretically that the noise level, defined as the root-mean-square of the resulting energy, was about 0.3 mm. Increasing the measurement time, and hence the accuracy of the estimator of the amplitudes, did not reduce this value. This noise level of 0.3 mm was also used in the continuous spectrum cases. It corresponds to an energy density of 0.9 mm^2/Hz in our case.

The uncertainties in the estimators of the spectral densities of the energy density spectra before decomposition are the normalized random errors, defined as

$$\epsilon_r = \frac{\sqrt{\text{variance(energy density)}}}{\text{energy density}} = \sqrt{\frac{2}{\text{d.o.f.}}} \tag{3.1}$$

in which d.o.f. is the number of degrees of freedom of the estimator [see for instance Bendat and Piersol (1986)]. The d.o.f. in the estimations of the low-frequency energy densities cannot be too high, because then the frequency bins become too broad, in which case the wave numbers of the low-frequency waves are not known accurately enough for the decomposition to make sense.

After decomposition, the uncertainties are not precisely known. Firstly, we do not know the influence of the CHPCA method on the uncertainties. This is due to the fact that the method uses the information of all wave-height meters to reduce the noise level, and the wave signals of different wave-height meters are by no means independent. Secondly, after the noise reduction, a least-squares method was used to obtain the different low-frequency wave components and again the wave signals from the different wave-height meters are not independent. So the standard techniques to obtain uncertainties of the spectral estimators cannot be applied.

We have determined approximate error estimates in the following way. The bound low-frequency wave spectral densities are predicted correctly from first-order energy–density spectra by full second-order theories such as that of Ottensen–Hansen (1978) and Laing (1986). (See for instance laboratory experiments by Kostense in 1984.) The errors in the estimates of the spectral densities of the bound waves are estimated to be the deviation from the calculated spectral densities from the theory of Laing (1986), based on the measured first-order energy–density spectrum. This first-order spectrum is taken equal to the measured spectrum around the peak frequency of the first-order waves. Of course these spectral densities contain their own uncertainties, but to obtain these spectra the degrees of freedom can be greatly increased. In this way we obtain standard deviations in the estimates of the energy–densities of 25%.

4. TEST OF THE NEW CONTROL SIGNAL

In this section, the new control signal is tested for bichromatic and continuous energy–density spectra of the first-order waves. The frequencies of the bichromatic first-order waves ranged from 0.6 to 0.8 Hz, with amplitudes ranging from 1.6 to 3.2 cm (see Table 1). This resulted in low-frequency wave amplitudes of about 2 mm. The continuous spectra are of the JONSWAP type with peak frequencies of 0.63 and 0.60 Hz and significant wave heights of 6 cm. In one of the test cases an artificial bar was placed on the beach. For all cases only the subharmonic part is tested. The criterion for a correct control signal is that outgoing free low-frequency waves should be absent up to second order.

4.1. *Bichromatic spectra*

Table 1 gives the test results for the bichromatic case. As stated in the preceding section the noise level is 0.3 mm. Because the non-linearity parameter ϵ (or μ) is about 0.1, the expected level of third-order effects is also of the order of 0.3 mm.

If the new generation method for the second-order waves is correct, the outgoing free wave signals must at most have amplitudes of those of the noise or due to third-order waves. In three of the eight tests, the amplitudes of the outgoing free waves are

Table 1. Test for bichromatic case. f1 and f2 are the frequencies of the first-order waves and a1 and a2 the corresponding amplitudes. "Laing" is the amplitude of the bound wave following Laing (1986). "Bound", "Free out" and "Free in" denote the amplitudes of the corresponding measured waves

High-frequency wave amplitudes				Low-frequency wave amplitudes			
f1 (Hz)	f2 (Hz)	a1 (cm)	a2 (cm)	Laing (mm)	Bound (mm)	Free out (mm)	Free in (mm)
0.6	0.7	1.77	2.97	1.9	1.9	0.0	1.5
0.6	0.7	2.79	2.12	2.1	2.5	0.5	1.7
0.7	0.8	1.73	3.12	1.4	1.4	0.2	1.2
0.7	0.8	2.77	2.21	1.6	1.8	0.6	1.4
0.6	0.75	1.65	3.10	1.7	1.5	0.3	1.4
0.6	0.75	2.77	2.25	2.1	2.1	0.5	1.8
0.6	0.8	1.55	3.18	1.6	1.4	0.3	1.2
0.6	0.8	2.68	2.37	2.0	2.1	0.3	0.7

above the 0.3 mm level but still of the same order, so we can conclude that the new control signal does work correctly for bichromatic spectra.

4.2. *Continuous spectra*

In Fig. 4 the measured energy–density spectrum is given for the JONSWAP case with a peak frequency of 0.63 Hz, a peak-enhancement factor of $\gamma = 3.3$ and a significant wave height of 0.06 m. The sample frequency in this case was 10 Hz. Figure 5 gives the corresponding low-frequency spectra of the different low-frequency waves. The frequency range is 0.05–0.35 Hz. The spectral densities of the incoming waves are divided by 10 to fit into the figure.

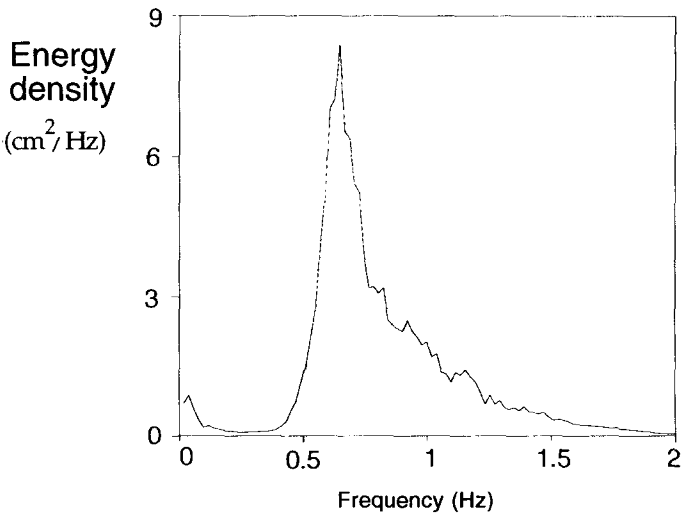

Fig. 4. Measured one-sided energy–density spectrum in the JONSWAP case, $\epsilon_r = 0.06$.

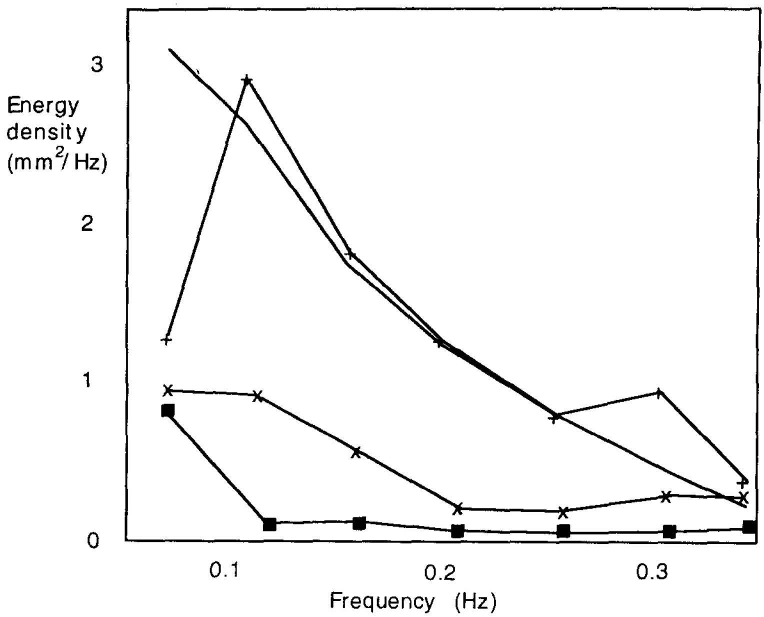

Fig. 5. One-sided low-frequency wave energy–density spectra. The solid line is the theoretical bound low-frequency wave spectrum (Laing, 1986). The other lines are the spectra of the decomposed waves: the line with the + for the outgoing bound waves, the line with the × for the outgoing free waves and the line with the boxes for the incoming free waves. The spectral densities of the incoming free waves are divided by 10 to fit into the figure.

The normalized random errors of the low-frequency wave signals before decomposition was 0.28 to obtain a frequency resolution of 0.01 Hz. We found that this value of the frequency resolution gave measured spectral densities of the bound waves which were closest to the theoretical values obtained from Laing (1986). After the decomposition, the spectral densities were averaged over the frequency intervals to reduce the sampling error. As noted before, the errors in the estimates of the spectral densities are of the order of 25%.

The energy densities of the outgoing free low-frequency waves do not exceed the noise level of 0.9 mm^2/Hz. To calculate the energy–density level of the third-order waves, we note that the non-linearity parameter ϵ (or μ) is about 0.1, so that the energy–density level of third-order waves, which is proportional to ϵ^2, is about 0.02 mm^2/Hz. So in this case, the noise level is much higher than the expected energy–density level of third-order waves. Outgoing low-frequency waves are also produced by reflection from the wave board of the incoming waves. We can use the measured reflection coefficients (Fig. 3) and the measured energy densities of the incoming waves to determine the reflected energy densities. We then find that only for the lowest frequencies (up to about 0.07 Hz) the reflected energy density is comparable with the noise level; for all other frequencies the reflected energy densities are much lower.

To gain more insight into the significance of the estimated energy–density levels of the outgoing free waves, we computed the coherence between the envelope of the high-frequency waves and the estimated outgoing free low-frequency waves. The envelope of the high-frequency waves was obtained from the Hilbert transform of the high-pass filtered time series [see Bendat and Piersol (1986)]. The 95% confidence interval on zero coherence was estimated by taking the d.o.f. of the low-frequency spectral estimates before the CHPCA multiplied by the number of points which were used in the averaging after the least-squares fit. This results in 65 d.o.f., which corresponds to a coherence of about 0.2. Note that the actual confidence interval will be somewhat above this value. As shown in Fig. 6, the coherences are not significantly different from zero, as would be expected if the low-frequency signals were noise. Of course this result does not prove that the outgoing low-frequency free-wave signal is actually due to noise, it gives only an indication that this can be the case.

In Fig. 7 the measured energy–density spectrum is given for a much broader spectrum of the first-order waves. The peak frequency is 0.60 Hz and the spectral width is slightly more than for a Pierson–Moskowitz spectrum. The significant wave height was 0.06 m and the sample frequency was 20 Hz. Figure 8 gives the corresponding spectra of the different low-frequency waves. Again, the spectral densities of the incoming waves are divided by 10 to fit into the figure.

The normalized random error was 0.41 for the low-frequency wave energy densities before decomposition to obtain again a frequency-bin width of 0.01 Hz. After decomposition we averaged over five frequency intervals to increase accuracy. The error in the spectral densities is again estimated to be 25%.

For most of the frequencies, the energy densities of the outgoing free waves do not exceed the noise level of 0.9 mm^2/Hz. The value of the non-linearity parameter can

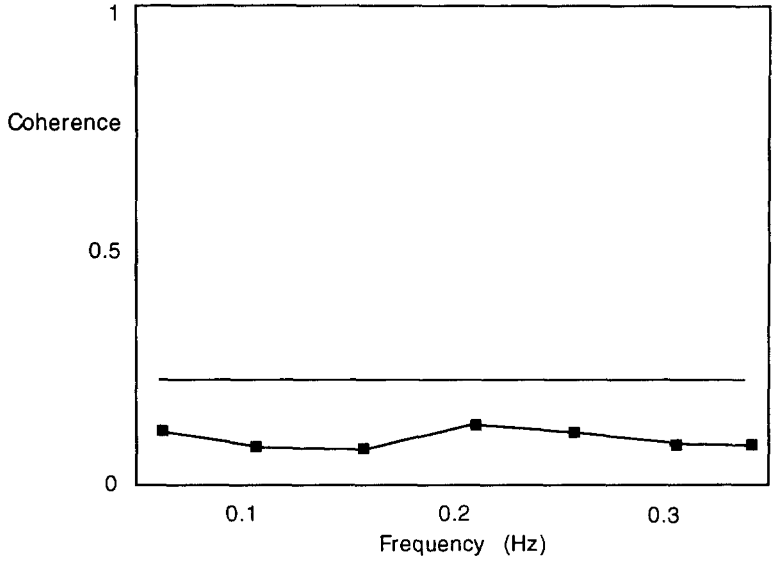

Fig. 6. Coherence between the high-frequency envelope and the outgoing free low-frequency waves for the JONSWAP case. The boxes are the estimates for the coherences and the drawn line indicates the 95% confidence interval on zero coherence.

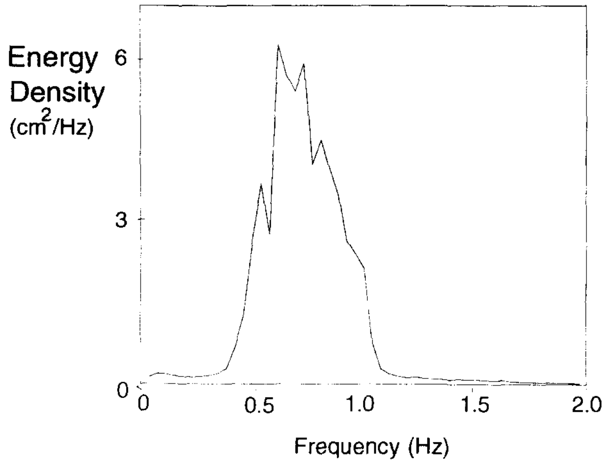

Fig. 7. Measured one-sided energy–density spectrum for the broad spectrum case, $\epsilon_r = 0.08$.

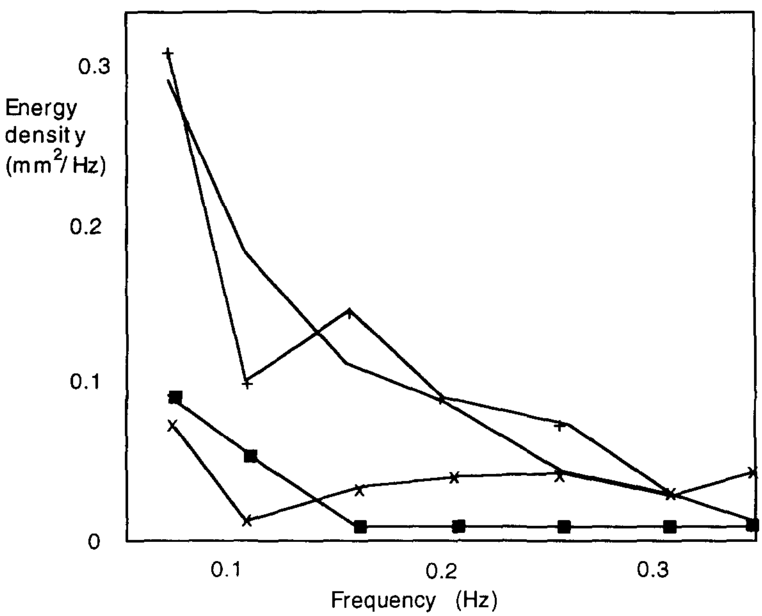

Fig. 8. One-sided low-frequency wave energy–density spectra. The solid line is the theoretical bound low-frequency wave spectrum (Laing, 1986). The other lines are the spectra of the decomposed wave components: the line with the + for the outgoing bound waves, the line with the × for the outgoing free waves and the line with the boxes for the incoming free waves. The spectral densities of the incoming free waves are divided by 10 to fit into the figure.

again be estimated as 0.1 so that the energy–density level of the third-order waves is again about 0.02 mm^2/Hz. So also in this case the noise level is much higher than the expected energy–density level of third-order waves. Reflection from the wave board of incoming waves produces only for the lowest frequencies an energy–density level of the reflected waves comparable to the noise level; for all other frequencies the energy densities from reflection are much lower.

In Fig. 9 the coherence between high-frequency wave envelope and outgoing low-frequency waves is given. The 95% confidence interval on zero coherence is obtained in the same way as above, which results in a threshold level of about 0.3. This time two points are on or a little above the 95% confidence interval on zero coherence but, as stated above, the coherence level of the confidence interval will be a little higher than 0.3. So also in this case we find that the outgoing free wave signals are probably due to noise.

5. CONCLUSIONS

A new time–domain method has been presented for the generation of random waves in a channel correct up to second-order in the wave slope. The derivation of the control signal for the wave board is based on multiple-scale perturbation-series analysis. In frequency–domain methods a convolution has to be performed, which is replaced in the time–domain method by a few multiplications. Therefore, the new method is computationally much more efficient than the conventional method.

The control signal was tested for the second-order subharmonic waves for bichromatic and continuous energy–density spectra of the first-order waves. The criterion for a

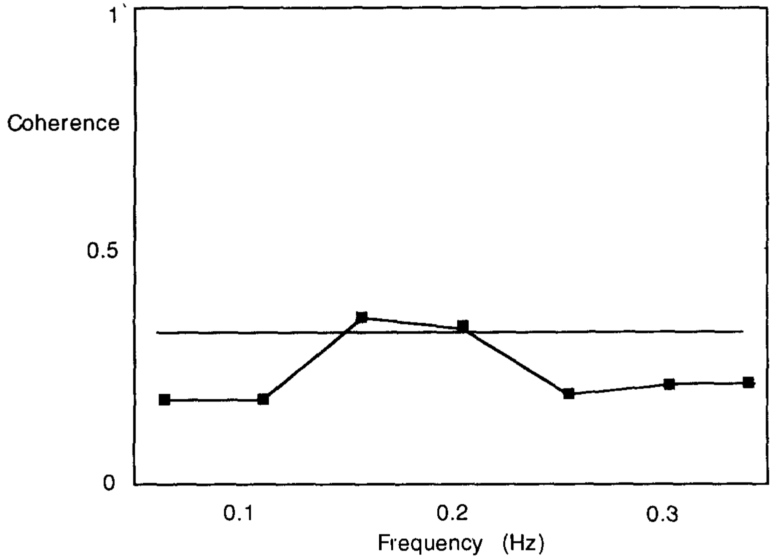

Fig. 9. Coherence between the high-frequency envelope and the outgoing free low-frequency waves for the broad spectrum case. The boxes are the estimates for the coherences and the drawn line indicates the 95% confidence interval on zero coherence.

correct control signal was that free low-frequency waves travelling away from the wave board must have amplitudes of third order at most.

The influence of noise in the data was greatly reduced by the CHPCA. The determination of the uncertainties in the spectral estimates could not be performed in a standard way. This is because more than one wave-height meter is used in the analysis and these wave-height-meter signals are no longer independent due to the principal-component analysis.

In the case of a bichromatic first-order energy–density spectrum, all tests showed free low-frequency waves propagating away from the wave board, which were at most of third order or of the same order as the noise level. So the new control signal for the wave board worked correctly in this case.

In the case of continuous first-order energy–density spectra two tests were performed, one with a JONSWAP-like spectrum and one with a broader spectrum. In both tests the energy–density levels of free low-frequency waves propagating away from the wave board were well below that of the bound low-frequency waves, which indicates that the new method is correct qualitatively. The noise level was too high to determine whether these free waves were of third order. However, the coherences of the first-order wave amplitude and the outgoing free low-frequency waves were not significant, which indicates that these estimated free-waves signals were probably due to noise.

An assumption in the new method is that the first-order energy–density spectrum is narrow banded. The test case with the JONSWAP-like spectrum certainly fulfils this requirement, but the other test was done with a first-order energy–density spectrum which was slightly broader than a Pierson–Moskowitz spectrum. However, both tests showed similar results, which indicates that the new method can also be applied to rather broad-banded spectra.

REFERENCES

Agnon, Y. and Mei, C.C. 1985. Slow-drift motion of a two-dimensional block in beam seas. *J. Fluid Mech.* **151,** 279–294.

Barthel, V., Mansard, E.P.D., Sand, S.E. and Vis, F.C. 1983. Group bounded long waves in physical models. *Ocean Engng* **10,** 261–294.

Bendat, J.S. and Piersol, A.G. 1986. *Random Data, Analysis and Measurement Procedures,* 2nd revised edition. John Wiley, New York.

Biésel, F. 1952. Equations générales au second ordre de la houle irrégulière. *La Houle Blanche* **7,** 372–376.

Dean, R.G. and Sharma, J.N. 1981. Simulation of wave systems due to nonlinear directional spectra. In *Proceedings of the International Symposium on Hydrodynamics in Ocean Engineering,* The Norwegian Institute of Technology, **2,** 1211–1222.

Foda, M.A. and Mei, C.C. 1981. Nonlinear excitation of long-trapped waves by a group of short swells. *J. Fluid Mech.* **111**, 319–345.

Hudspeth, R.T. and Sulisz, W. 1991. Stokes drift in two-dimensional wave flumes. *J. Fluid Mech.* **230,** 209–229.

Klopman, G. and van Leeuwen, P.J. 1990. An efficient method for the reproduction of nonlinear random waves. In *Proceedings of the 22nd Coastal Engineering Conference,* Delft, ASCE.

Kostense, J.K. 1984. Measurements of surf beat and set down beneath wave groups. In *Proceedings of the 22nd Coastal Engineering Conference,* Houston, ASCE.

Laing, A.K. 1986. Nonlinear properties of random gravity waves in water of finite depth. *J. Phys. Oceanogr.* **16,** 2013–2030.

Longuet-Higgins, M.S. and Stewart, R.W. 1962. Radiation stress and mass transport in gravity waves, with applications to 'surf beat'. *J. Fluid Mech.* **13,** 481–504.

Mei, C.C. 1983. *The Applied Dynamics of Ocean Surface Waves.* John Wiley, New York.

Nayfeh, A.H. 1981. *Introduction to Perturbation Techniques.* John Wiley, New York.

Ottesen Hansen, N-E. 1978. Long period waves in natural wave trains. *Prog. Rep., Inst. Hydrodyn. Hydraulic Engng., Technical University Denmark* **46,** 13–24.

Preisendorfer, R.W. 1988. *Principal Component Analysis in Meteorology and Oceanography*. Elsevier, Amsterdam.

Sand, S.E. 1982. Long wave problems in laboratory models. *J. WatWay, Port, Coastal Ocean Engng* **108,** (WW4) 492–503.

Sand, S.E. and Mansard, E.P.D. 1986. The reproduction of higher harmonics in irregular waves. *Ocean Engng* **13,** 57–83.

Tatavarti, R.V.S.N., Huntley, D.A. and Bowen, A.J. 1988. Incoming and outgoing wave interactions on beaches. In *Proceedings of the 21st Coastal Engineering Conference, ASCE,* Malaga, 136–150.

Tucker, M.J., Challenor, P.G. and Carter, D.J.T. 1984. Numerical simulation of a random sea: a common error and its effect upon wave-group statistics. *Appl. Ocean Res.* **6,** 118–122.

Wallace, J.M. and Dickinson, R.E. 1972. Empirical orthogonal representation of time series in the frequency domain Part I: Theoretical considerations. *J. Appl. Meteorol.* **11,** 887–892.